Manuscript prepared for Nat. Hazards Earth Syst. Sci. Discuss.
with version 2014/05/30 6.91 Copernicus papers of the LaTeX class copernicus.cls.
Date: 8 August 2015

TITAN2F: a pseudo-3-D model of 2-phase debris flows

G. Córdoba[1], M. F. Sheridan[2], and E. B. Pitman[3]

[1]Universidad de Nariño, Pasto, Colombia
[2]Center for Geohazards Studies and Department of Geology, University of Buffalo, Buffalo, NY 14260, USA
[3]Center for Geohazards Studies and Department of Mathematics, University of Buffalo, Buffalo, NY 14260, USA

Correspondence to: G. Córdoba (gcordobaguerrero@gmail.com)

Kurzfassung

Debris flows, avalanches, landslides, and other geophysical mass flows can contain $O(10^6$–$10^{10})\,\mathrm{m}^3$ or more of material. These flows commonly consist of mixture of soil and rocks with a significant quantity of interstitial fluid. They can be tens of meters deep, and their runouts can extend many kilometers. The complicated rheology of such a mixture challenges every constitutive model that can reasonably be applied; the range of length and timescales involved in such mass flows challenges the computational capabilities of existing models. This paper extends recent efforts to develop a depth averaged "thin layer" model for geophysical mass flows that contain a mixture of solid material and fluid. Concepts from the engineering community are integrated with phenomenological findings in geoscience, resulting in a theory that accounts for the principal solid and fluid forces as well as interactions between the phases, across a wide range of solid volume fractions. A principal contribution here is to present drag and phase interaction terms that comport with the literature in geosciences. The program predicts the evolution of the concentration and dynamic pressure. The theory is validated with data from one dimensional dam break solutions and it is verified with data from artificial channel experiments.

1 Einleitung

Globally there are about 50 volcanoes that erupt every year. During the past century tens of thousands of people have been killed by volcanic flows and hundreds of thousands forced from their homes (Tilling, 1996; The-Committee-on-Natural-Disasters, 1991; U.S.-Geodynamics-Committee, 1994). Two-phase mass flows containing water and solid particles, called lahars, are common in volcanic regions. They can be initiated by several mechanisms. A volcanic explosion can be accompanied by large plumes and pyroclastic flows consisting of rock and gas that race along the surface of the mountain at speeds as high as $100\,\mathrm{m}$ per second (Sheridan, 1979). The hot ash can melt snow, creating a muddy mixture that knock down trees and entrain rocks and boulders into the flow. Cotopaxi Volcano in Ecuador is an example of a volcano that has produced many large lahars by this process in the past (Pistolesi et al., 2013). Crater lakes on

volcanoes are another source of mud flows, a recent example being the 2007 lahar of Ruapehu in New Zealand (Procter et al., 2010). A third mechanism for initiating lahars is intense rainfall on hillsides that are devoid of vegetation and exposures of loose material like clay soils or volcanic ash. An example of this type of lahar is the 1998 mudflow at Casita Volcano in Nicaragua that occurred during Hurricane Mitch and caused hundreds of deaths (Sheridan et al., 1999). Lahars can carry constituent particles that are typically from clay to boulder size and can propagate tens of kilometers before coming to rest (Procter et al., 2010). As solid particle sediment out of the flowing mass the resulting deposits can be up to one hundred meters thick (Legros, 2002). However, the typical deposits left after a debris flow passes are on the scale of meters.

In order to develop a complete mathematical model of mud and debris flows, two principal challenges must be overcome: rheology, and scale. First, constitutive relations must be developed to describe granular material including clays, sands, pebbles and rocks, with interstitial water. Second, a computational method must be developed that extends over six orders of magnitude, as clay diameters are $O(10^{-6}\ m$ and boulders are $O(1)\ m$. Neither of these challenges can be fully met at this time. This paper tries to strike a balance between fidelity to the physics of mass flows and computational feasibility. We describe a modeling effort that draws on the wisdom from engineering and geoscience, to postulate constitutive theory and fluid-solid interaction effects, and, through a depth averaging process, results in a system of equations that is computationally tractable.

The modeling effort here has its origins the pioneering work of Savage and Hutter (1989). They began with mass and momentum balance laws based on a Coulomb constitutive description of dry granular material. By scaling and depth averaging, they develop a "thin layer" model for granular flows down inclines. Flow over general topography was addressed in Gray et al. (1999), Patra et al. (2005), and Pudasaini and Hutter (2003). Comparison of thin layer model results to historic flows is presented in Sheridan et al. (2005). In Hutter et al. (2003), the appropriateness of these thin layer models is considered, for several different types of geophysical flows. Much of the modeling effort is summarized in Pudasaini and Hutter (2007).

Iverson and his co-workers (Iverson, 1997; Iverson and Denlinger, 2001) argue that the presence of interstitial fluid fundamentally alters the behavior of geophysical flows, and fluid effects

should be included in the constitutive behavior of the flowing material. Starting with equations of mixture theory (Bedford and Drumheller, 1983) and through a careful examination of experiments, these papers developed a system of mass and momentum balance laws for the mixture. Unfortunately in this development an equation for the motion of pore fluid was not readily available. Instead, based on experimental data, a transport equation for the fluid was postulated.

A different approach, based on a fully three dimensional model of two phase flows, can be found in Meruane et al. (2010) and Dartevelle (2004).

Pitman and Le (2005) rigorously developed a two phase thin layer model of fluid and granular material. They begin with a fully three dimensional model of two phase flows, based on model equations in engineering (Jackson, 2000). The model equations are scaled and depth averaged. The resulting system of equations is not complete, and closure assumptions are required. With these assumptions, the mathematical system is shown to be hyperbolic under common conditions, and thus well posed (see Pelanti et al., 2008). The model of Pitman and Le (2005) includes a drag term, which is the only term describing the interaction of the two phases; the coefficient of drag must be fitted to experiments. That model assumes the fluid is inviscid, and that there is no frictional dissipation in the fluid phase at the basal surface. Both of these features, which are reasonable in bench-scale fluidized bed experiments, are suspect for large mass flows. In order to address some of the shortcomings of the Pitman and Le (2005) model, this paper reconsiders the model equations proposed by them and proposes a revision that better represents two phase geophysical flows, for example accounting for the friction at the wall of the fluid phase and no longer assuming a constant volumetric fraction of solids. Related work can be found in Valentine and Wohletz (1989) and Dobran (1991).

A different approach to modeling mud flows employ a visco-plastic constitutive assumptions (Mei at al, 2001; Coussot, 1997); see also Ancey (2006) and Balmforth and Craster (1999). In these papers, the choice of a visco-plastic flow model drives the subsequent derivation, as well as the required parameter-fitting necessary for the constitutive relations. The process of depth averaging a visco-plastic flow is always difficult. The interface between yielding and non-yielding material is itself a free surface that must be determined. This attribute requires the use of multiple layers in the model system, with all the resulting complexity.

2 Model derivation

This paper uses a similar framework to that developed in Pitman and Le (2005). However, a complete set of model equations for a granular phase and for a fluid phase are written. Phase interaction terms are modeled, and scaling of all terms suggests simplifications that can be made. Depth averaging and closure assumptions completes the derivation.

A note on sign convention: in soil mechanics it is common to consider compressive stresses as positive; by contrast, in fluid mechanics, as an increase in pressure results in a reduction of the volume, compression is negative. We caution the reader to observe the sign convention in the equations below.

2.1 Fundamental assumptions

The fundamental theory of two phase flows used here can be found in Dobran (1991) and Jackson (2000). In two space dimensions we consider a thin layer of granular material (s) and interstitial fluid (f), each of constant specific density ρ^{s} and ρ^{f}, respectively, flowing over a smooth basal surface, b. Erosion and deposition are neglected. Along the basal surface, we define a Cartesian coordinate system $Oxyz$, with origin O defined so the Oxy is tangent to the basal surface, with the x direction the downstream direction, and Oz is in the normal direction. Writing $\boldsymbol{v}$, $\boldsymbol{u}$ for the velocities of the solid and fluid constituents, respectively, φ for the solid volume fraction and φ^f for the fluid volume fraction. We assume the mass is fully saturated, so the sum of the solid and fluid volume fractions adds to one ($\varphi^f = 1 - \varphi$). When writing equations in component form, we use subscripts to denote the component of the vectors, and superscripts the phase of the flow (either solids or fluid).

Mass conservation for the two constituent phases may be written as in Anderson and Jackson (1967):

$$\partial_t \rho^{\mathrm{s}} \varphi + \nabla \cdot (\rho^{\mathrm{s}} \varphi \boldsymbol{v}) = 0 \tag{1}$$

$$\partial_t \rho^{\mathrm{f}} (1-\varphi) + \nabla \cdot (\rho^{\mathrm{f}} (1-\varphi) \boldsymbol{u}) = 0 \tag{2}$$

The momentum equations are:

$$\partial_t(\rho^{\mathrm{s}}\varphi\boldsymbol{v}) + \nabla\cdot(\rho^{\mathrm{s}}\varphi\boldsymbol{v}\boldsymbol{v}) = \nabla\cdot T^{\mathrm{s}} + f^{\mathrm{s}} + \rho^{\mathrm{s}}\varphi\boldsymbol{g} \tag{3}$$

$$\partial_t(\rho^{\mathrm{f}}(1-\varphi)\boldsymbol{u}) + \nabla\cdot(\rho^{\mathrm{f}}(1-\varphi)\boldsymbol{u}\boldsymbol{u} = \nabla\cdot T^{\mathrm{f}} + f^{\mathrm{f}} + \rho^{\mathrm{f}}(1-\varphi)\boldsymbol{g} \tag{4}$$

Here T^{s}, T^{f} are the stress tensors for the solid and fluid, and f^{s}, f^{f} the interaction force between the phases. We must postulate constitutive relations and an equation for the interphase force, to close the system. Jackson (2000) presents an argument for separating buoyancy from other interphase force terms (such as drag or virtual mass), and for properly accounting for buoyancy in a field with fluid pressure variations. Similar modeling can be found in Neri et al. (2003), Neri et al. (2007), Dobran (2001), Dobran et al. (1993) and Valentine and Wohletz (1989). Neglecting capillarity, virtual mass and lift, we postulate

$$\begin{aligned} f^{\mathrm{s}} &= -\varphi\nabla T^{\mathrm{f}} + D(\boldsymbol{v}-\boldsymbol{u}) \\ f^{\mathrm{f}} &= -f^{\mathrm{s}} \end{aligned} \tag{5}$$

Here the total fluid stress is $T^{\mathrm{f}} = -P^{\mathrm{f}} + \tau^{\mathrm{f}}$, where P^{f} is the fluid pressure and τ^{f} is the viscous contribution to the fluid stress. The drag term exchanges momentum between the phases, with a coefficient D that is phenomenological; Wallis (1969), Ergun (1952), Gidaspow (1994), Fan and Zhu (1998), Dobran (2001), Panneerselvan et al. (2007), and Mazzei and Lettieri (2007) among other sources, suggest values. As $\varphi \to 1$ the effect of fluid forces becomes less important, relative to frictional forces. When $\varphi \to 0$, the drag vanishes. Following Mazzei and Lettieri (2007), we set

$$D \;=\; \frac{3}{4}C_{\mathrm{d}}\frac{\rho^{\mathrm{f}}\varphi|\boldsymbol{v}-\boldsymbol{u}|}{d}(1-\varphi)^{-\beta} \tag{6}$$

where d is the mean particle diameter, β is a constant related to the constant n in Ricardson–Zaki equation (Khan and Richardson, 1989). According to Mazzei and Lettieri (2007), this constant equals 2.80 either when $R_{e_p} \to 0$ or $R_{e_p} \to \infty$, thus we use $\beta = 2.80$ in Eq. (6). Finally, he drag coefficient is assumed to be constant $C_{\mathrm{d}} = 1$.

2.2 Scaling

The characteristic thickness of the flowing granular material is H and the characteristic length L. We scale x and y by L, and z by H, time by the free fall time $\sqrt{L/g}$, and the x, y and z velocities by $\sqrt{Lg}$ and $\frac{H}{L}\sqrt{Lg}$, respectively. The stresses are scaled by $\rho^{\mathrm{s}} gH$ for the solids phase and $\rho^{\mathrm{f}} gH$ for the fluid phase. After scaling the mass balance equations are unchanged. Several terms in the momentum equations contain the factor $\epsilon = H/L$ which is small; $\epsilon \approx 0.01-0.001$ is not uncommon (Iverson and Denlinger, 2001). Writing x, y, z for x_1, x_2, x_3, the solid momentum balance equations become

$$\begin{aligned}
&\partial_t(\varphi v_x) + \partial_x(\varphi v_x v_x) + \partial_y(\varphi v_y v_x) + \partial_z(\varphi v_z v_x) \qquad (7)\\
&= \partial_x \epsilon T^{\mathrm{s}}_{xx} + \partial_y \epsilon T^{\mathrm{s}}_{xy} + \partial_z T^{\mathrm{s}}_{xz} - \epsilon \frac{\rho^{\mathrm{f}}}{\rho^{\mathrm{s}}} \varphi \partial_x T^{\mathrm{f}}_{xx}\\
&- \epsilon \frac{\rho^{\mathrm{f}}}{\rho^{\mathrm{s}}} \varphi \partial_y T^{\mathrm{f}}_{xy} - \frac{\rho^{\mathrm{f}}}{\rho^{\mathrm{s}}} \varphi \partial_z T^{\mathrm{f}}_{xz} + \frac{D}{\rho^{\mathrm{s}}}(v_x - u_x) + \varphi g_x\\
&\partial_t(\varphi v_y) + \partial_x(\varphi v_x v_y) + \partial_y(\varphi v_y v_y) + \partial_z(\varphi v_z v_y) \qquad (8)\\
&= \partial_x \epsilon T^{\mathrm{s}}_{xy} + \partial_y \epsilon T^{\mathrm{s}}_{yy} + \partial_z T^{\mathrm{s}}_{yz} - \epsilon \frac{\rho^{\mathrm{f}}}{\rho^{\mathrm{s}}} \varphi \partial_x T^{\mathrm{f}}_{xy}\\
&- \epsilon \frac{\rho^{\mathrm{f}}}{\rho^{\mathrm{s}}} \varphi \partial_y T^{\mathrm{f}}_{yy} - \frac{\rho^{\mathrm{f}}}{\rho^{\mathrm{s}}} \varphi \partial_z T^{\mathrm{f}}_{yz} + \frac{D}{\rho^{\mathrm{s}}}(v_y - u_y) + \varphi g_y\\
&\epsilon(\partial_t(\varphi v_z) + \partial_x(\varphi v_x v_z) + \partial_y(\varphi v_y v_z) + \partial_z(\varphi v_z v_z)) \qquad (9)\\
&= \partial_x \epsilon T^{\mathrm{s}}_{xz} + \partial_y \epsilon T^{\mathrm{s}}_{yz} + \partial_z T^{\mathrm{s}}_{zz} - \epsilon \frac{\rho^{\mathrm{f}}}{\rho^{\mathrm{s}}} \varphi \partial_x T^{\mathrm{f}}_{xz}\\
&- \epsilon \frac{\rho^{\mathrm{f}}}{\rho^{\mathrm{s}}} \varphi \partial_y T^{\mathrm{f}}_{yz} - \frac{\rho^{\mathrm{f}}}{\rho^{\mathrm{s}}} \varphi \partial_z T^{\mathrm{f}}_{zz} + \epsilon \frac{D}{\rho^{\mathrm{s}}}(v_z - u_z) + \varphi g_z
\end{aligned}$$

Note that components of gravity have been scaled by the magnitude $|g|$, so (g_x, g_y, g_z) is a unit vector.

With the same scaling, the fluid momentum balance equations become

$$\begin{aligned}
&\partial_t((1-\varphi)u_x) + \partial_x((1-\varphi)u_x u_x) + \partial_y((1-\varphi)u_y u_x) + \partial_z((1-\varphi)u_z u_x) \\
&= \partial_x \epsilon(1-\varphi)T^{\mathrm{f}}_{xx} + \partial_y \epsilon(1-\varphi)T^{\mathrm{f}}_{xy} + \partial_z(1-\varphi)T^{\mathrm{f}}_{xz} - \frac{D}{\rho^{\mathrm{f}}}(v_x - u_x) + (1-\varphi)g_x \qquad (10) \\
&\partial_t((1-\varphi)u_y) + \partial_x((1-\varphi)u_x u_y) + \partial_y((1-\varphi)u_y u_y) + \partial_z((1-\varphi)u_z u_y) \\
&= \partial_x \epsilon(1-\varphi)T^{\mathrm{f}}_{xy} + \partial_y \epsilon(1-\varphi)T^{\mathrm{f}}_{yy} + \partial_z(1-\varphi)T^{\mathrm{f}}_{yz} - \frac{D}{\rho^{\mathrm{f}}}(v_y - u_y) + (1-\varphi)g_y \qquad (11) \\
&\epsilon(\partial_t((1-\varphi)u_z) + \partial_x((1-\varphi)u_x u_z) + \partial_y((1-\varphi)u_y u_z) + \partial_z((1-\varphi)u_z u_z)) \\
&= \partial_x \epsilon(1-\varphi)T^{\mathrm{f}}_{xz} + \partial_y \epsilon(1-\varphi)T^{\mathrm{f}}_{yz} + \partial_z(1-\varphi)T^{\mathrm{f}}_{zz} - \epsilon\frac{D}{\rho^{\mathrm{f}}}(v_z - u_z) + (1-\varphi)g_z \qquad (12)
\end{aligned}$$

In summary, then, the proposed equation system consists of the solid volume fraction φ, the three solid velocities $\boldsymbol{v}$, and three fluid velocities $\boldsymbol{u}$. These variables evolve according to the six momentum balance laws for the species, and the mass conservation relations for each species.

2.3 Constitutive assumptions and boundary conditions

The upper surface of the flowing mass at $F_h(x, y, t) = 0$ is assumed to be a material surface and stress free. At the base of the mass, material is assumed to flow tangent to the basal surface $F_{\mathrm{b}} = 0$, and to satisfy a sliding friction law. For the solid constituent, this friction relation specifies that the shear traction and the normal stress are proportional: $S|_{F_{\mathrm{b}}} = -\mathrm{sgn}(v)\, N|_{F_{\mathrm{b}}} \tan(\phi_{\mathrm{bed}})$, where ϕ_{bed} is the basal friction angle and the $-\mathrm{sgn}(v)$ specifies that the shear traction opposes motion.

We now discuss constitutive relations. A Coulomb constitutive relation is postulated for the material. The Coulomb law is a nonlinear relation among the components of $\mathbf{T}^{\mathrm{s}}$, and stipulated that material deforms when the total stress reaches yield, $||\mathrm{dev}(\mathbf{T}^{\mathrm{s}})|| = \kappa\, \mathrm{tr}(\mathbf{T}^{\mathrm{s}})$, where $\mathrm{dev}(\mathbf{T}^{\mathrm{s}}) = \mathbf{T}^{\mathrm{s}} - \frac{1}{2}\mathrm{tr}(\mathbf{T}^{\mathrm{s}})\mathbf{I}$ is the stress deviator, $\mathrm{tr}(\mathbf{T}^{\mathrm{s}})$ is the trace of the stress (the sum of the diagonal components), $\mathbf{I}$ is the identity tensor, and κ is a material parameter, and that as deformation occurs, the stress and strain-rate tensors are aligned. That is, the alignment condition

specifies $\mathrm{dev}(\mathbf{T}^{\mathrm{s}}) = \lambda \mathrm{dev}(\mathbf{V})$, where the strain-rate $\mathbf{V} = -\frac{1}{2}(\nabla \boldsymbol{v} + \nabla \boldsymbol{v}^{\dagger})$ and $\dagger$ denotes the transpose. To avoid a switching between plastic and non-plastic behavior, we assume the solid material is everywhere in plastic yield.

The full Coulomb relations are too complex to be used here. Two simplifications are proposed. First, at the basal surface the boundary condition ensures proportionality and alignment of the tangential and normal forces; we assume the same proportionality and alignment holds throughout the thin flowing layer of material. Written in components ij, this implies ${T_{\mathrm{ij}}}^{\mathrm{s}} = \nu_{\mathrm{ij}} {T_{zz}}^{\mathrm{s}}$, where the proportionality constant ν is a function of ϕ_{bed}. Second, following Rankine (1957) and Terzaghi (1936), an earth pressure relation is assumed for the diagonal stress components, $\nu_{\mathrm{ii}} = k_{\mathrm{ap}}$, or ${T_{xx}}^{\mathrm{s}} = k_{\mathrm{ap}} {T_{zz}}^{\mathrm{s}}$, where

$$k_{\mathrm{ap}} = 2\frac{1 \pm [1 - \cos^2(\phi_{\mathrm{int}})[1 + \tan^2(\phi_{\mathrm{bed}})]]^{\frac{1}{2}}}{\cos^2(\phi_{\mathrm{int}})} - 1.$$

Here ϕ_{int} is the internal friction angle and the choice of the plus or minus sign depends on whether flow is locally expanding (the active state, with $\nabla \cdot \boldsymbol{v} > 0$, and the $-$ sign) or contracting (the passive state, with $\nabla \cdot \boldsymbol{v} < 0$, and the $+$ sign).

For the fluid, the stress terms in 10 should be such that in case of $\varphi_s \to 0$ the equations agrees with the pure fluid depth averaged equations.

For pure water, the shear stress at wall can be approached by Chow (1969)

$$\tau_w = \rho^f g R_h S_f - 1.$$

where S_f is the slope friction and R_h is the hydraulic ratio. Note that for shallow water problems $R_h \to h$. There are several approaches for the slope friction, thus for the shear stress at wall as well. For example, **?** use the empirical Manning approach, whereas **?** and **?** use the Chezy equation. Both Manning and Chezy appropaches pose numerical problmes when $h \to 0$. Thus we use use the Darcy equation Guo (1995); Xu (2004):

$$\tau_{xz} = -\rho^{\mathrm{f}} C_f u_x^2$$

where

$$C_f = \rho^f \frac{f_r}{8}$$

is the Chezy coefficient. The friction coefficient f_r depends on the Reynolds number and the roughness of the channel (k_s).

3 Depth averaging

The final step in the derivation is a depth averaging of the mass and momentum balance equations. In this and the following sections we will use the same notation used by Savage and Hutter (1989). If $h(x,y,t)$ is the unsteady surface of the flow and $b(x,y)$ is the terrain surface, for some function f, we compute

$$\frac{1}{|h-b|} \int_{b(x,y)}^{h(x,y,t)} f(x,y,z,t)\,\mathrm{d}z = \overline{f}.$$

where $h-b$ is the flow depth at a point (x,y) and time t. Repeated use of the Leibnitz rule is made to interchange integration and differentiation, and boundary conditions are employed to evaluate terms at b and h. In addition, several approximations must be made during the depth averaging process. In what follows, we only briefly sketch the depth averaging process, noting as appropriate those places where approximations are made. Pitman and Le (2005) provides an estimation of the errors typically made by these assumptions.

The terms of order ϵ are assumed small and we hope to drop all such terms from the model. However Savage and Hutter (1989) argues that diagonal contributions to the solid stress must be retained. Because there is no preferential downslope direction in our applications, and the flow

direction may change during a flow, we retain the stress terms in both the x and y directions, dropping only $O(\epsilon)$ terms in the z direction; see the discussion in Iverson and Denlinger (2001). Other $O(\epsilon)$ terms are dropped.

Mass balance equation

As ρ^s and ρ^f are constants, equations 1 can be reduced to

$$\nabla \cdot (\varphi \boldsymbol{v} + (1-\varphi)\boldsymbol{u}) = 0 \, .$$

which says that the volume-weighted mixture flow is divergence free. This equation is integrated from $z = b$ to $z = h$:

$$\int_b^h \nabla \cdot (\varphi \boldsymbol{v} + (1-\varphi)\boldsymbol{u}) \, \mathrm{d}z = 0. \tag{13}$$

Use the Leibniz rule to interchange differentiation and integration. The upper free surface $F_h = 0$ is a material surface for the mixture, so, following Savage and Hutter (1989) and Pitman and Le (2005), at $z = h(x, y, t)$

$$\begin{aligned} &\partial_t(\varphi h + (1-\varphi)h) + (\varphi v_x + (1-\varphi)u_x)\partial_x h \\ &+ (\varphi v_y + (1-\varphi)u_y)\partial_y h - (\varphi v_z + (1-\varphi)u_z) \; = \; 0 \, . \end{aligned} \tag{14}$$

At the basal surface $F_\mathrm{b} = 0$, the flow is tangent to the fixed bed and the bed is fixed in time, thus we can drop in 14 the terms in ∂_t, taking into account that at the surface $z = b(x, y)$ (Pitman and Le, 2005)

$$(\varphi v_x + (1-\varphi)u_x)\partial_x b \qquad +(\varphi v_y + (1-\varphi)u_y)\partial_y b - (\varphi v_z + (1-\varphi)u_z) = \; 0 \, . \tag{15}$$

In arriving at these equations, we have ignored sedimentation, entrainment, and infiltration of fluid into the bed.

Using these formulae and algebraic manipulation,the depth averaged equation for the total mass of the solid and fluid can be written

$$\partial_t \hat{h} + \partial_x(\hat{h}(\overline{\varphi v_x} + \overline{(1-\varphi)u_x})) + \partial_y(\hat{h}(\overline{\varphi v_y} + \overline{(1-\varphi)u_y})) = 0. \tag{16}$$

In writing this equation, the depth averaged velocities are $\hat{h}\overline{v_x} = \int_b^h v_x \, \mathrm{d}z$, with a similar expression for the volume fraction $\overline{\varphi}$ and the other velocity components, and as in Savage and Hutter (1989), $\hat{h} = h - b$.

z momentum

Observe that, upon setting $\epsilon \to 0$ in the fluid z momentum equation, we find the fluid to be hydrostatic:

$$\partial_z T^{\mathrm{f}}_{zz} = g_z.$$

Integrating and imposing boundary conditions, we find

$$T^{\mathrm{f}}_{zz}(x,y,z) \;=\; -g_z[h-z], \tag{17}$$

and the average

$$\overline{T}^{\mathrm{f}}_{zz}(x,y) \;=\; -\frac{1}{2} g_z \hat{h}. \tag{18}$$

In the same manner, for the solid z momentum we find equation for an effective stress:

$$\partial_z T^{\mathrm{s}}_{zz} + \frac{\rho^{\mathrm{f}}}{\rho^{\mathrm{s}}} \varphi \partial_z T^{\mathrm{f}}_{zz} = \varphi g_z.$$

Substituting,

$$\partial_z T^{\mathrm{s}}_{zz} \;=\; \left(1 - \frac{\rho^{\mathrm{f}}}{\rho^{\mathrm{s}}}\right) g_z \varphi$$

Thus the normal solid stress in the z direction at any height is equal to the (buoyancy) reduced weight of the solid material overburden.

In scaling these equations, the z velocities have been dropped. Of course neglecting motion in the z direction is a central component of a thin layer theory. Furthermore, any contribution to the z momentum from fluid shearing – terms such a $T^{\mathrm{f}}_{xz}, T^{\mathrm{f}}_{yz}$ – are dropped due to scaling. This observation suggests that only pressure contributions to the fluid stress are important, an assumption we will make below, albeit with a modification at the basal surface.

x and y momentum

We now must depth average the remaining momentum equations. The nonlinearity of these equations present difficulties in formulating a depth averaged theory, complicate the derivation, and in several places, it is necessary to take the depth average of products of terms. When necessary we approximate the required closure relation, for example as $\overline{\varphi f} \approx \overline{\varphi}\,\overline{f}$ (Savage and Hutter, 1989; Pitman and Le, 2005).

Consider first the equation for the motion of the solid phase. The left-hand side of the x momentum equation (7) can be written

$$\mathrm{LHS} = \partial_t \varphi v_x + \partial_x \varphi v_x + \partial_y \varphi v_x v_y + \partial_z \varphi v_x v_z \ .$$

Depth average and use boundary conditions to find

$$\int_b^h \mathrm{LHS}\,\mathrm{d}z \ = \ \partial_t \int_b^h \varphi v_x \,\mathrm{d}z + \partial_x \int_b^h \varphi v_x^2 \,\mathrm{d}z + \partial_y \int_b^h \varphi v_x v_y \,\mathrm{d}z \tag{19}$$

Now depth average the right hand side of (7):

$$\int_b^h \text{RHS}\,\mathrm{d}z = \underbrace{-\int_b^h (\epsilon\partial_x T^{\text{s}}_{xx} + \epsilon\partial_y T^{\text{s}}_{xy} + \partial_z T^{\text{s}}_{xz})\,\mathrm{d}z}_{\text{(i)}} \tag{20}$$

$$\underbrace{-\frac{\rho^{\text{f}}}{\rho^{\text{s}}}\int_b^h \epsilon\varphi\partial_x T^{\text{f}}_{xx}\,\mathrm{d}z}_{\text{(ii)}} + \underbrace{\frac{D}{\rho^{\text{s}}}(v_x - u_x)}_{\text{(iii)}} + \int_b^h \varphi g_x\,\mathrm{d}z\ .$$

In order to proceed, several assumptions are made:

- This equation governs the motion of the solid phase, and we assume the upper free surface for the mixture is a free surface for both of the individual phases.
- The drag term $\frac{D}{\rho^{\text{s}}}(v_x - u_x)$ is highly nonlinear and a correct depth average is all but impossible to calculate. We postulate that a experiments could fit an averaged phenomenological drag of a similar form. As seen in equation 6 we assume a drag coeficient $C_d = 1$. In addition, we use the typical mean particle for lahars $d = 1\ \ mm$ (Schmid, 1981)
- The earth pressure relation for the solid phase is employed. That is, the basal shear stresses are assumed to be proportional to the normal stress:

  $$T^{\text{s}}_{iz} = -\frac{v_i}{||\boldsymbol{v}||}\tan(\phi_{\text{bed}})T^{\text{s}}_{zz} \equiv \alpha_{*z}T^{\text{s}}_{zz},$$

  where i can be either x or y, and the velocity ratio enforces that friction opposes motion in the designated direction (Savage and Hutter, 1989; Patra et al., 2005) The α notation will provide a convenient shorthand that we use in other places. Likewise the diagonal stresses are taken to be proportional to the normal solid stress

  $$T^{\text{s}}_{ii} = k_{\text{ap}}T^{\text{s}}_{zz} \equiv \alpha_{ii}T^{\text{s}}_{zz}\ .$$

Finally, following Iverson and Denlinger (2001), xy shear stresses are determined by a Coulomb relation

$$T^{\mathrm{s}}_{xy} = -\mathrm{sgn}(\partial_y v_x)\sin(\phi_{\mathrm{int}})k_{\mathrm{ap}}T^{\mathrm{s}}_{zz} \equiv \alpha_{xy}T^{\mathrm{s}}_{zz} \ ,$$

where the sgn function ensures that friction opposes straining in the (x, y) plane.

– For the fluid phase, the basal shear stresses are assumed to be proportional to the square of the depth averaged velocities (Guo, 1995; Xu, 2004):

$$T^{\mathrm{f}}_{iz} = \rho^{\mathrm{f}} C_f u_i ||\boldsymbol{u}|| \ ,$$

where C_f is the Chezy coefficient, which depends on the friction coefficient f_r (see equation 13. A physical approach for this coefficient is the Colebrook–White equation (Colebrook and White, 1937), which for rough channels can be approximated as:

$$\frac{1}{\sqrt{f_{\mathrm{r}}}} = -2\log_{10}\left(\frac{k_{\mathrm{s}}}{14.8R_{\mathrm{h}}}\right) \ ,$$

where k_{s} is the roughness of the channel and R_{h} is the hydraulic radii, which for shallow water problems can be approached as the depth of the flow ($R_{\mathrm{h}} \to h$). Equation 21 is logarithmic, thus large uncertainties in k_s result only in small variations in C_f (swaffield and Bridge, 1983). Transport and Road Research Laboratory (1975) proposes values of k_s for different materials and channel types. We use $k_s = 1 \ mm$ for channels in volcanic environments. Therefore, here C_r will depend on the flow depth $\hat{h}$, ρ^{f} and the fluid velocity u_i. Note that this is a physical approach for T^f_{iz}, which does not depend on empiric.

For pure fluids, the diagonal stresses and shear stress are zero.

From Leibniz's rule and the stress computations above, we find

$$\text{(ii)} = -\epsilon \frac{\rho^{\mathrm{f}}}{\rho^{\mathrm{s}}} \int_b^h \varphi \partial_x T^{\mathrm{f}}_{xx} \, \mathrm{d}z =$$

$$-\epsilon \frac{\rho^{\mathrm{f}}}{\rho^{\mathrm{s}}} \overline{\varphi} [\partial_x \left(\frac{\hat{h}^2}{2} (-g^z) \right) + \hat{h}(-g_z) \partial_x b]. \tag{21}$$

Now using the fluid and solid stress relation $\overline{T}^{\mathrm{s}}_{zz} = \left(1 - \frac{\rho^{\mathrm{f}}}{\rho^{\mathrm{s}}}\right) \overline{\varphi} \overline{T}^{\mathrm{f}}_{zz}$, term (i) is approximated as:

$$\text{(i)} = -\epsilon \int_b^h \partial_x \alpha_{xx} T^{\mathrm{s}}_{zz} \, \mathrm{d}z - \epsilon \int_b^h \partial_y \alpha_{xy} T^{\mathrm{s}zz} \, \mathrm{d}z - \int_b^h \partial_z \alpha_{xz} T^{\mathrm{s}}_{zz} \, \mathrm{d}z \tag{22}$$

$$= -\epsilon [\partial_x \int_b^h \alpha_{xx} T^{\mathrm{s}}_{zz} \, \mathrm{d}z - \alpha_{xx} T^{\mathrm{s}}_{zz}|_{z=h} \partial_x h + \alpha_{xx} T^{\mathrm{s}}_{zz}|_{z=b} \partial_x b] - \epsilon [\partial_y \int_b^h \alpha_{xy} T^{\mathrm{s}}_{zz} \, \mathrm{d}z$$

$$- \alpha_{xy} T^{\mathrm{s}}_{zz}|_{z=h} \partial_y h + \alpha_{xy} T^{\mathrm{s}}_{zz}|_{z=b} \partial_y b] - \alpha_{xz} [T^{\mathrm{s}zz}|_{z=h} - T^{\mathrm{s}zz}|_{z=b}] \, .$$

The upper free surface is stress free, so all terms involving $T^{\mathrm{s}}_{zz}|_{z=h}$ vanish. The expression for (i) becomes

$$\text{(i)} = -\epsilon \left(1 - \frac{\rho^{\mathrm{f}}}{\rho^{\mathrm{s}}}\right) \partial_x \left(\hat{h} \alpha_{xx} \overline{\varphi} \overline{T}^{\mathrm{f}}_{zz} \right) - \epsilon \left(1 - \frac{\rho^{\mathrm{f}}}{\rho^{\mathrm{s}}}\right) \partial_y \left(\hat{h} \alpha_{xy} \overline{\varphi} \overline{T}^{\mathrm{f}}_{zz} \right)$$

$$+ \left(1 - \frac{\rho^{\mathrm{f}}}{\rho^{\mathrm{s}}}\right) (-\epsilon \alpha_{xx} \partial_x b - \epsilon \alpha_{xy} \partial_y b + \alpha_{xz})(-g_z) \hat{h} \overline{\varphi} \, . \tag{23}$$

Note that the factor $(-g_z)$ originates in the evaluation and depth averaging of the fluid stress; in typical flows, this factor is positive.

Combining all terms yields a solids x momentum equation:

$$\partial_t\left(\hat{h}\overline{\varphi v_x}\right)+\partial_x\left(\hat{h}\overline{\varphi v_x v_x}\right)+\partial_y\left(\hat{h}\overline{\varphi v_x v_y}\right)=-\frac{\epsilon}{2}\left(1-\frac{\rho^{\mathrm{f}}}{\rho^{\mathrm{s}}}\right)\partial_x(\alpha_{xx}\hat{h}^2\overline{\varphi}(-g_z)) \tag{24}$$
$$-\frac{\epsilon}{2}\left(1-\frac{\rho^{\mathrm{f}}}{\rho^{\mathrm{s}}}\right)\partial_y(\alpha_{xy}\hat{h}^2\overline{\varphi}(-g_z))+\left(1-\frac{\rho^{\mathrm{f}}}{\rho^{\mathrm{s}}}\right)(-\epsilon\alpha_{xx}\partial_x b-\epsilon\alpha_{xy}\partial_y b+\alpha_{xz})\hat{h}\overline{\varphi}(-g_z)$$
$$-\frac{\epsilon}{2}\frac{\rho^{\mathrm{f}}}{\rho^{\mathrm{s}}}\overline{\varphi}\partial_x(\hat{h}^2(-g_z))-\epsilon\frac{\rho^{\mathrm{f}}}{\rho^{\mathrm{s}}}\hat{h}\overline{\varphi}(-g_z)\partial_x b+\left(\frac{\overline{D}}{\rho^{\mathrm{s}}}\right)(\overline{u_x}-\overline{v_x})+\hat{h}\overline{\varphi}g^x.$$

The y solid momentum equation can be derived in a similar fashion.

The equation for the fluid motion presents fewer difficulties. The depth averaged x momentum equation takes the form

$$\partial_t\left(\hat{h}\overline{\varphi^{\mathrm{f}}}\overline{u_x}\right)+\partial_x\left(\hat{h}\overline{u_x}\overline{\varphi^{\mathrm{f}}}\overline{u_x}\right)+\partial_y\left(\hat{h}\overline{\varphi^{\mathrm{f}}}\overline{u_x u_y}\right) \tag{25}$$
$$=-\frac{1}{2}\epsilon\partial_x\hat{h}^2\overline{\varphi^{\mathrm{f}}}(-g_z)-\left(\frac{\overline{D}}{\rho^{\mathrm{s}}}\right)(\overline{u_x}-\overline{v_x})+\hat{h}\overline{\varphi^{\mathrm{f}}}g_x+\overline{\varphi^{\mathrm{f}}}C_f u_x||\boldsymbol{u}||.$$

Where $\overline{\varphi^{\mathrm{f}}}=1-\overline{\varphi}$. Again, the fluid y momentum equation has a similar form. Note that if $\overline{\varphi^{\mathrm{f}}}\to 1$ Eq. (25) becomes the typical shallow water approach of hydraulics (Chow, 1969) (Kowalski, 2008 describes how debris flows reduces to a shallow water flow as solid volume fraction vanishes).

As noted above, we solve for volume fractions (φ), thus the bulk density can be calculated from:

$$\rho=\rho^{\mathrm{s}}\varphi+\rho^{\mathrm{f}}(1-\varphi) \tag{26}$$

Then, we obtain the dynamic pressure p from:

$$p=\frac{1}{2}\rho\overline{\boldsymbol{v}}^2 \tag{27}$$

where $\overline{\boldsymbol{v}}$ is the mixture averaged velocity of the flow (Fan and Zhu, 1998)

$$\overline{\boldsymbol{v}} = \frac{\rho^s \overline{v}\varphi + \rho^f \overline{u}(1-\varphi)}{\rho} \tag{28}$$

where $\overline{v} = \sqrt{v_x^2 + v_y^2}$ and $\overline{u} = \sqrt{u_x^2 + u_y^2}$ are the speeds of each phase.

The use of the impacting dynamic pressure information on structures and living beings allows to estimate levels of damage, as in Valentine (1998), Valentine et al. (2011), and Jones (2012), useful for vulnerability analysis.

Numerical solution

This system of equations is then solved using the finite volume method, whose solution provides results of the velocity field, flow depth and the volumetric concentration of solids at the center of the each finite volume computational grid.

To solve the balance laws, we use the parallel, adaptive mesh, Godunov solver developed by Davis (1988) already implemented in Patra et al. (2005) and Pitman and Le (2005). The adaptive meshing is used as well, which allows to have very fine grids where indicators show high gradients, and coarser grids where low gradients are detected. The time step is adjusted from a CFL condition (Courant et al., 1928). The complexity of the equation system results in typical time steps of the order of 10^{-4}. However, the maximum time step allowed was reduced from 10^{-1} s used within Titan2D to 10^{-3} s to ensure stability. As consequence of this small time step, Titan2F become a computationally expensive tool.

The numerical solution of the above set of equations presents strong numerical sensitivity to small changes and Digital Elevation Model (DEM) errors and the quality of that maps. The DEMS can have regions where elevations are not well defined, they can have crossed contour levels or even infinite holes. Abrupt terrain changes, both actual or DEM artifacts, cause computations of gradients and curvatures to become unstable. In order to avoid such a numerical problems patching and intelligent smoothing of the DEMs was needed.

From the hyperbolicity analysis done by Pitman and Le (2005), we try to ensure hyperbolicity imposing a minimum $\hat{h}_{min} = 10^{-5}\ \ m$, a maximum $\varphi_{max} = \varphi_{pc}$ correspondent to a maximum packing concentration of 0.65 and a minimum $\varphi_{min} = 10^{-8}$. This constrains makes the program very stable if a good DEM is used.

The needed initial conditions are the location of the pile, its geometry, the volumetric solid concentration and initial velocity. There is no inflow condition implemented yet. The bed and internal friction are set internally as fixed values. Nevertheless, both of this parameters can affect k_{ap}. The red line in Figure 1 shows how K_{ap} changes with ϕ_{bed} for *any* value of ϕ_{int} (Note that Williams et al. (2008) shows that Titan2D results are not strongly affected by ϕ_{int}). The black line in the same figure shows how k_{ap} evolves when the fix value of $\phi_{bed} = 40^o$, used in the program, is multiplied by $0 < \varphi < 0.65$. We set internally $\phi_{int} = 42^o$ as well. Then, we use in the evaluation of k_{ap}, the result of the multiplication $\varphi \times \phi_{bed}$ and $\varphi \times \phi_{int}$ instead of ϕ_{bed} and ϕ_{int} respectively.

Differences with Pitman and Le (2005) model

There are five major differences between the present paper and Pitman and Le (2005):

1. In Pitman and Le (2005), mass and momentum conservation laws are derived for the solid material and for the phase averaged mixture of solid and fluid, whereas here the final model presents mass and momentum equations for both individual phases.

2. Any two phase model system must postulate several phenomenological functions, such as inter-phase drag coefficient. In the present derivation these functions are better adapted to geophysical flows whose fluid phase corresponds to water and the solid phase are rounded solid particle. The drag is calculated from an expression valid for the whole range of Reynolds numbers. It only needs the mean particle diameter of the flow as a parameter. We use a typical mean particle diameter of lahars.

3. The volumetric particle concentration is no longer a fixed parameter, which in our approach is calculated for every time step and grid point. This mean that instead of having

constant φ like in equations 3.2 in Pitman and Le (2005) or simply not accounted for, like in the depth averaged fluid mass and momentum balance equations 3.27 and 3.28 in Pitman and Le (2005), we include the variable φ within all derivatives and depth averaged equations. Thus, in regions when the particle concentration vanishes, the solid phase role in the equation system vanishes as well. In that way, the equation system becomes the typical hydraulic shallow water approach, which does not happen in Pitman and Le (2005).

4. We account for the fluid stresses at wall. We use a physical approach that only needs the roughness of the channel and the flow depth. The last term is calculated by the program at every time step, whereas that the former is set as fixed value.

5. The only input parameters needed by the program are the location of the pile of material, its volume and the volumetric solids concentration. The friction coefficients are no longer needed as input as they are automatically adjusted according to the evolution of the volumetric fraction of solids across the grid and time. The bed and internal friction are set in such way that when the volumetric fraction of solids tends to an assumed maximum packing concentration ($\varphi = 0.65$), both internal and bed frictions tends to the values used in that cases in Titan2D (see Sheridan et al. (2005) and Williams et al. (2008) for ranges of values).

4 Validation and verification

In order to validate and verify the proposed approach, we did a series of tests using a one dimensional approach of the proposed system of equations. First, we test the consistency of the results verifying the expected symmetries. Then we used an exponentially decaying topography with and without obstacles (bumps). They show expected features like how the mathematical model can show a reflected wave when the bump was big enough or the flow splitting in a reflected dense part and bump overpass by a very dilute flow. In addition we verify the predictions with two dimensional experimental measurements done by Liu (1996) and Iverson et al. (2010).

Verification of the accuracy of the code was done with analytical solutions of the Dam Break problem and with several experimental results. Among them, we check the deposited pattern predicted by the program with the results shown by Liu (1996). The prediction of the arrival time and the flow depth profile was compared with the experimental results shown by Iverson et al. (2010) from his recent work done on his large channel facility.

Analytical solutions for shallow water problems are scarce. Only one dimensional analytical approaches are available in the literature, especially for the well known Dam Break problem (e.g. Dressler, 1954; Mangeney et al., 2000; Fernandez-Feira, 2006; Ancey et al., 2008; Wrachien and Mambretti, 2009). Unfortunately, analytical solutions for geo-mass flows are almost impossible to find due to the complexity of the non-linear partial differential equations (Pudasaini and Hutter, 2007). Such solutions can be obtained only in special cases like the similarity based solutions proposed by Savage and Hutter (Savage and Hutter, 1989) for dry avalanches. In our test we use the solution proposed by Fernandez-Feira (2006) for the Dam Break problem on an incline for pure water. In our program we assume $\varphi^{s} \rightarrow 0$. Figure 2 shows a comparison of the Titan2F prediction with this analytical solution. The statistical *t*-test shows that there is no statistical difference between the analytical solutions and the 1D prediction. That test shows that about 70% of the predictions of Titan2F can explain the analytical solution. At least for the one dimensional case, the program successfully reproduces analytical solutions for different initial conditions down to very low particle concentrations (less than $1\,\%$). However, it can be noted in Figure 2 that the 1D version of the program tends to over-estimate the front advance of the flow, at least in the initial parts of its evolution.

Liu (1996) performed several experiments for geo-mass flows in an inclined channel. He modified the initial volume, the channel slope and the particle concentration to find the final size of the debris flows measured by their resulting width and length. We reproduced experimental final width and length after the simulation reached the same time corresponding to the duration reported by Liu. Figure 3 shows the correspondence of the model with the experiments for (a) the width of the deposit and (b) the length. A Pearson correlation shows that $90\,\%$ of the experimental data for the deposit length can be explained with the predictions of Titan-Two-Phase, whereas $80\,\%$ of the data for the deposit width can be explained by the predictions of the

program. This illustrates the high accuracy of the program in predicting the deposit characteristics for different initial volumes and high initial solid concentrations.

The experiments performed by Iverson and co-workers (Iverson et al., 2010) done on a $95\,\mathrm{m}$ long artificial channel was used to verify the accuracy of the predictions of the flow front arrival time and the temporal evolution of the flow depth. These flows were unsteady and nonuniform. Iverson et al. (2010) show time series data for several measured properties: flow thickness, pore pressure, basal normal stress and arrival time of the front. Raw data sent to us by Dr. Iverson were used to test the Two-Phase-Titan prediction concerning time evolution of the flow depth and arrival times at the check points located at 32 and $66\,\mathrm{m}$ distance from the lock. As shown in Figures 4 and 5, the arrival time and the temporal evolution of the predicted depth fits very well within the confidence interval of the experiments. In both of the cases, Titan2F tends to over-estimate the flow depth just after the arrival of the front. This is probably an effect of the slight difference in the shape of the initial pile, as the free surface of the numerical pile follows the same slope of the channel, whereas the actual free surface within the lock is horizontal.

The range of concentrations that the program cope with, are from $\varphi_s = 10^{-8}$ (almost pure water) to $\varphi_s = 0.65$ (maximum packing concentration). Finally, as expected, the program predicts high particle concentrations at the front of the flow and low particle concentrations at the tail of the flow (at some cases, even near pure water concentrations, or $\varphi \to 0$), as can be seen in Fig. 6 where a longitudinal solids particle distribution predicted by Titan2F is shown. The predictions fits with Iverson et al. (2010) observation that the tail of the flow remains very watery. Using predicted concentration of solids, the density is assessed (Eq. 26) and together with the speed of the flow, the dynamic pressure distribution is calculated as well (Eq. 27). Figure 7 shows longitudinal and cross distributions of the dynamic pressures after $32\,\mathrm{s}$ simulation. As the flow velocity at lateral limits of the flow from the end of the channel are very low, the dynamic pressure shows to be low as well. Knowledge of the dynamic pressure information is of vital importance in risk analysis as structural damage and risk for human life can be assessed from it.

Verification with actual mud flows has been done as well, showing very good fit with field data. For example, Sheridan et al. (2011) shows that the Titan2F predictions are within $10\,\%$

of the data shown by Procter et al. (2010) for the highly channeled mud flow at Ruapehu, New Zealand. In addition, the theory was tested against field data assessed by Williams et al. (2008) for the 2006 Vazcun creek lahar at Tungurahua volcano, Ecuador, as shown by Cordoba et al. (2015), where Titan2F predictions about velocity are within $10\,\%$ and within $15\,\%$ for the measured super-elevation.

5 Fazit

In this paper we present a new computational two phase tool for lahar hazard assessment that has no constrains on initial volumetric particle concentration. The program computes space–time evolution of the particle concentration, flow depth, velocity field and dynamic pressure at each point of the computational grid.

The model is valid for two phase flows whose phases consist in solids and water. However, the phenomenological approach used for the interphase drag model assumes an average diameter of the solids, which mean individual boulders or particles cannot be tracked. In addition, the model is depth averaged, assuming thin layer and shadow water approaches. Thus, our model correctly predicts the dynamic of gravity driven flows providing the depth averaged values for the particle concentration, flow and phases velocities and flow depth in a three dimensional topography. In order to model other kind of geophysical mass flows, adjustments to the code must be done, for example pyroclastic flows can be modeled if the flow density of the fluid phase is appropriately addressed (eg. thermocoupled air density using ideal gas law and an additional equation for temperature).

The proposed mathematical approach allows to study the whole range of flow behavior. Regions with almost pure fluid to regions of friction dominated flows are correctly described by the algorithm. Using this information, dynamic pressure is deduced, which becomes a very useful tool for risk assessment.

The highly non-linear coupled equation system makes the time step very small. The use of this new tool on natural terrains or detailed Digital Elevation Models (DEMs) requires higher

computational power than the one provided for home PCs. The use of a high velocity Work Station with multiple cores is advised.

Important processes that are not addressed by this tool include the effect of turbulence, incorporation of solid material from the bed of the channel, and incorporation of water into the flow from existing water bodies. Nevertheless, this two-phase flow is an important step forward in forming an acceptable computational model for simulating a hazardous natural phenomena. Currently, we are applying this tool for real lahar hazard assessments like in Cordoba et al. (2015).

The Supplement related to this article is available online at doi:10.5194/nhessd-0-1-2015-supplement.

Gustavo Córdoba, Michael Sheridan and Bruce Pitman developed the mathematical approach of the model. Gustavo Córdoba did the coding.

Acknowledgements. The authors wish to thank the economic support provided by the National Science Foundation Grant EAR 711497 aimed to the developing of Two-Phase-Titan. We also want to thanks Ramona Stefanescu, Abani Patra, Dinesh Kumar and Keith Dalbey from University of Buffalo for the useful discussions about this development, and to Dr. Richard Iverson from USGS who sent us the raw data of his experiments. The Universidad de Nariño, Colombia, allowed the mobility of Cordoba to assume the post-doctoral position at the University of Buffalo (2008–2010) where the mathematical approach and coding of the beta version was developed, and later gave him the necessary dedication time for this research. Finally, we thanks for the suggestions of the anonymous referees. who help us in the substantial improvement of the paper.

Literatur

Ancey, C.: Plasticity and geophysical flows: a review, J. Non-Newton Fluid, 142, 4–35, 2006.

Ancey, C., Iverson, R., Rentschler, M., and Denlinger, R.: An exact solution for ideal dam-break floods on steep slopes, Water Resour. Res., 44, W01430, doi:10.1029/2007WR006353, 2008.

Anderson, T. B. and Jackson, R.: A fluid mechanical description of fluidized beds: equations of motion, Ind. Eng. Chem. Fund., 6, 527–539, 1967.

Balmforth, N. J. and Craster, R. V.: A consistent thin-layer theory for Bingham plastics, J. Non-Newton Fluid, 84, 65–81, 1999.

Bedford, A. and Drumheller, D. S.: Recent advances: theories of immiscible and structured mixtures, Int. J. Eng. Sci, 21, 863–960, 1983.

Xu, K. : The gas-kinetic scheme for shallow water equations, Journal of Hydrodynamics, Proceedings of the Conference of Global Chinese Scholars on Hydrodynamics, 73–76, Shangai, China, 11-14 July, 2006.

Chow, V.: Open Channel Hydraulics, McGraw Hill, New York, 1969

Colebrook, C. and White, C.: Experiments with fluid friction in Roughened pipes, P. R. Soc. London, 161, 367–381, 1937.

U.S.-Geodynamics-Committee: Mount Rainier: Active Cascade Volcano, National Academic Press, Washington, D.C., 1994.

Córdoba, G., Villarosa, G., Sheridan, M. F., Viramonte, J. G., Beigt, D., and Salmuni, G.: Secondary lahar hazard assessment for Villa la Angostura, Argentina, using Two-Phase-Titan modelling code during 2011 Cordón Caulle eruption, Nat. Hazards Earth Syst. Sci., 15, 757–766, doi:10.5194/nhess-15-757-2015, 2015.

Courant, R., Friedrichs, K., and Lewy, H.: On the partial difference equations of mathematical physics, Math. Ann., 100, 32–74, 1928.

Coussot, P.: Mudflow Rheology and Dynamics, IAHR Monograph Series, Balkema, 1997.

Dartevelle, S.: Numerical modeling of geophysical granular flows: 1. A comprehensive approach to granular rheologies and geophysical multiphase flows, G-cubed-Geochemistry-Geophysics-Geosystems, 5, Q08003, doi:10.1029/2003GC000636, 2004.

Davis, S. F.: Simplified second order Godunov-type methods, SIAM J. Sci. Stat. Comp., 9, 445-473, 1988.

Dobran, F.: Theory of structured multiphase mixtures, Lect. Notes Phys., Volume 372, Springer, Berlin, Deutschland, 1991.

Dobran, F.: Volcanic Processes: Mechanisms in Material Transport, Kluwer Academic, NY, 2001.

Dobran, F., Neri, A., and Macedonio, G.: Numerical Simulation of collapsing volcanic columns, J. Geophys. Res., 98, 4231–4259, 1993.

Dressler, R. F.: Comparison of theories and experiments for hydraulic dam break waves, Proc. Int. Assoc. of Scientific Hydrology Assemblee Generale, 38, 319–328, 1954.
Ergun, S.: Fluid flow through packed columns, Chem. Eng. Prog., 49, 89-94, 1952.
Fan, L. and Zhu, C.: Principles of Gas-Solid Flows, Cambridge CB2 2RU, Cambridge, 1998.
Fernandez-Feira, R.: Dam-break flow for arbitrary slopes on the bottom, J. Eng. Math., 54, 319–331, 2006.
Gidaspow, D.: Multiphase Flow and Fluidization, Academic Press, New York, 1994.
Hutter, K., Wang, Y., and Pudasaini, S. P.: The Savage-Hutter Avalanche Model: How far can it be pushed?, Preprint, NI03072-GPF, Isaac Newton Institute for Mathematical Sciences, Cambridge, UK, 2003.
Gray, J. M., Wieland, M., and Hutter, K.: Gravity-driven free surface flow of granular avalanches over complex basal terrain, P. Roy. Soc. Lond. A, 455, 1841–1874, 1999.
Guo, Z.: Velocity-depth coupling in shallow-water flows, J. Hydrol. Eng., 121, 717–724, 1995.
Iverson, R. M.: The physics of debris flows, Rev. Geophys., 35, 245–296, 1997.
Iverson, R. M. and Denlinger, R. P.: Flow of variably fluidized granular material across three-dimensional terrain 1: Coulomb mixture theory, J. Geophys. Res., 6, 537–552, 2001.
Iverson, R. M., Logan, M., LaHusen, R. G., and Berti, M.: The perfect debris flow? Aggregated results from 28 large-scale experiments, J. Geophys. Res., 115, F03005, doi:10,1029/2009FJ001514, 2010.
Jackson, R.: The Dynamics of Fluidized Particles, Cambridge Monographs on Mechanics, Cambridge University Press, Cambridge, UK, 2000.
Jones, N.: Damage of plates due to impact, dynamic pressure and explosive loads, Lat. Am. J. Solids Stru., 10, 767–780, 2012.
Khan, A. R. and Richardson, J. F.: Fluid-particle interactions and flow characteristics of fluidized and settling beds ans settling suspensions of spherical particles, Chem. Eng. Commun., 78, 111–130, 1989.
Kowalski, J.: Two-Phase Modeling of Debris Flows, PhD thesis, Eidgenossische Technische Hochschule (ETH), Zurich, Switzerland, 135 pp., 2008.
Le, L.: New Models for geophysical mass flows. PhD Thesis. Department of Mathematics. State University of New York at Buffalo, 2006.
Legros, F.: The mobility of long runout landslides, Eng. Geol., 63, 301–331, 2002.
Liu, X.: Size of a debris flow deposition: model experiment approach, Environ Geol., 28, 70–77, 1996.
Mangeney, A., Heinrich, P., and Roche, R.: Analytical solution for testing debris avalanche numerical models, Pure Appl. Geophys., 157, 1081–1096, 2000.

Mazzei, L. and Lettieri, P.: A drag force closure for uniformly dispersed fluidized suspensions, Chem. Eng. Sci., 62, 6129–6142, 2007.
Mei, K., Liu, F., and Yuhi, M.: Mud flow – slow and fast, Geomorph. Fluid Mech., 22, 548–577, 2001.
Meruane, C., Tamburrino, A., and Roche, O.: On the role of the ambient fluid on gravitational granular flow dynamics, Journal of Fluid Mechanics, 648, 381–404, 2010.
Neri, A., Ongaro, T. E., Macedonio, G., and Gidaspow, D.: Multiparticle simulation of collapsing volcanic columns and pyroclastic flows, J. Geophys. Res., 108, 508–531, 2003.
Neri, A., Ongaro, T. E., Menconi, G., Vitturu, M., Cavazzoni, C., Erbacci, G., and Baxter, P.: 4D simulation of explosive eruption dynamics at Vesuvius, Geophys. Res. Lett., 34, 1–7, 2007.
Panneerselvan, R., Savithri, S., and Surender, G. D.: CFD based investigations on hydrodynamics and energy dissipation due to solid motion in liquid fluidized bed, Chem. Eng. J., 132, 159–171, 2007.
Patra, A., Bauer, C., Nichita, C., Pitman, E., Sheridan, M., Bursik, M., Rupp, B., Webber, A., Stinton, A., Namikawa, L., and Renschler, C.: Parallel adaptive numerical simulation of dry avalanches over natural terrain, J. Volcanol. Geoth. Res., 139, 1–21, 2005.
Pelanti, M., Bouchut, F., and Mangeney, A.: A Roe-type scheme for two-phase shallow granular flows over variable topography, Math. Model. Numeric. Analy., 42, 851–885, 2008.
Pistolesi, M., Cioni, R., Rosi, M., Cashman, K. V., Rossotti, A., and Aguilera, E.: Evidence for lahar-triggering mechanisms in complex stratigraphic sequences: the post-twelfth century eruptive activity of Cotopaxi Volcano, Ecuador, B. Volcanol., 75, 698, , 2013.
Pitman, E. B. and Le, L.: A two-fluid model for avalanche and debris flows, Philos. T. R. Soc., 363, 1573–1601, 2005.
Procter, J. N., Cronin, S. J., Fuller, I. C., Sheridan, M., Neall, V. E., and Keys, H.: Lahar hazard assessment using Titan2D for an alluvial fan with rapidly changing geomorphology: Whangaehu River, Mt. Ruapehu, Geomorphology, 116, 162–174, 2010.
Pudasaini, S. P. and Hutter, K.: Rapid shear flows of dry granular material down curved and twisted channels, J. Fluid Mech., 495, 193–208, 2003.
Pudasaini, S. P. and Hutter, K.: Avalanche Dynamics, Springer-Verlag, Berlin, 2007.
Rankine, W. J. M.: On the stability of loose earth, Philos. T. R. Soc. Lond., 147, 9–27, 1957.
Savage, S. B. and Hutter, K.: The motion of a finite mass of granular material down a rough incline, J. Fluid Mech., 199, 177–215, 1989.
Schmid, R., Descriptive nomenclature and classification of pyroclastic deposits and fragments: recommendations of the IUGS subcommision on systematics of igneous rocks. Geology, 9, 41-43., 1981.
Sheridan, M.: Emplacement of pyroclastic flows: a review, Geol. S. Am S., 180, 125–136, 1979.

Sheridan, M.: Pyroclastic block flow from the September 1976, eruption of La Soufrière Volcano, Guadaloupe, Bull. Volcanol., 43-2, 397–402, 1980.
Sheridan, M. and Malin, M.: Application of computer-assisted mapping to volcanic hazard evaluation of surge eruptions: Vulcano, Lipari and Vesuvius, J. Volcanol. Geoth. Res., 17, 187–202, 1983.
Sheridan, M. F., Bonnard, C., Carreno, R., Siebe, C., Strauch, W., Navarro, M., Calero, J. C., and Trujillo, N. B.: Rockfall/avalanche and breakout flow of Casita Volcano, Nicaragua, Landslide News, 12, 2-4, 1999.
Sheridan, M. F., Stinton, A. J., Patra, A. K., Bauer, A. C., Nichita, C. C., and Pitman, E. B.: Evaluating TITAN2D mass-flow model using the 1963 Little Tahoma Peak avalanches, Mount Rainier, Washington., J. Volcanol. Geoth. Res., 139, 89–102, 2005.
Sheridan, M., Córdoba, G., Pitman, E., Cronin, S., and Procter, J.: Application of a wide-ranging two-phase Debris Flow Model to the 2007 Crater Lake break-out lahar at Mt. Ruapehu, New Zealand, American Geophysical Union Fall Meeting, San Francisco (CA), 5–9 December 2011, abstract V53E-2691, 2011.
Swaffield, J.A., and Bridge, S., Applicability of the Colebrook-White formula to represent frictional losses in partially filled unsteady pipeflow. J. of research of the National Bureau of Standards, 88, 389-393, 1983.
Terzaghi, K.: The shearing resistance of saturated soils and the angle between planes of shear, Proc. 1st Int. Conf. Soil Mech., June 22-26, 1936, Cambridge, Mass., 54–56, 1936.
Transport and Road Research Laboratory, A guide for engineers to the design of storm sewer systems. Roadnote 35, 1975
The-Committee-on-Natural-Disasters: The Eruption of Nevado del Ruiz Volcano, Colombia, South America, November 13, 1985, Natural Disaster Studies, V4, National Academic Press, Washington, D.C., 1991.
Tilling, R. I.: Volcanoes, U.S. Geological Survey, U.S. Government Peinting Office, Washington, D.C., 1996.
Valentine, G.: Damage to structures by pyroclastic flows and surges, inferred from nuclear weapons effects, JVGR, 87, 117–140, 1998.
Valentine, G. and Wohletz, K.: Numerical models of plinian eruptions columns and pyroclastic flows, J. Geophys. Res., 94, 1867–1887, 1989.
Valentine, G., Doronzo, D., Dellino, P., and Tullio, M.: Effects of volcano profile on dilute pyroclastic density currents: numerical simulations, Geology, 39, 947–950, 2011.
Wallis, G. B.: One-Dimensional Two-Phase Flow, McGraw Hill, NY, 1969.

Williams, R., Stinton, A. J., and Sheridan, M. F.: Evaluation of the Titan2D two-phase flow model using an actual event: case study of the 2005 Vazcún Valley Lahar, J. Volcanol. Geoth. Res., 177, 760–766, 2008.

Wrachien, D. and Mambretti, S.: Dam-Break Problems, Solutions and Case Studies, WITpress, Southampton, UK, 2009.

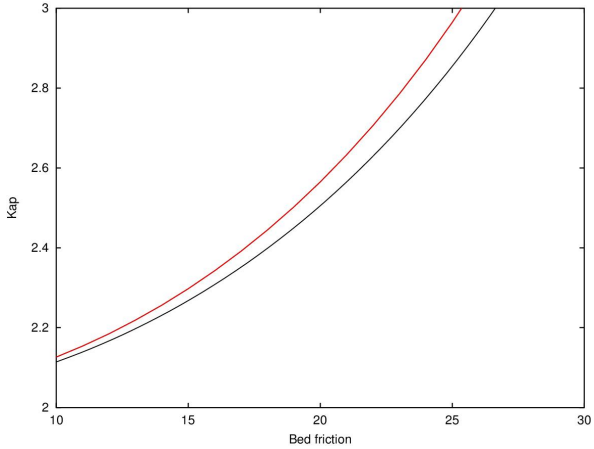

Abb. 1. Effect on k_{ap} due to changes in ϕ_{bed} and $42^o \times \varphi$ given a fix ϕ_{int}. The black line shows the changes related with ϕ_{bed} for *any* fixed ϕ_{int}. The red line shows the relation k_{ap} with $42^o \times \varphi$, used within the program.

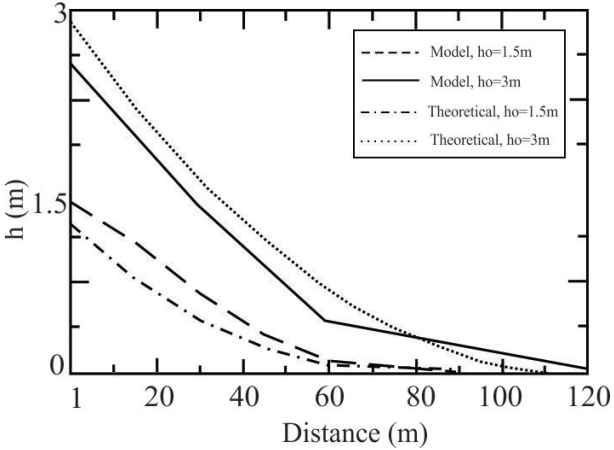

Abb. 2. Dam-break 1-D problem. Evolution of the flow front depth with distance. The figure shows the result of the theoretical solution and the results from the numerical model for two initial conditions ($h_o = 3\ m$ and $h_o = 1.5\ m$). The statistical *t*-test shows that there is no statistical significant difference between the analytical solution and the predictions of Titan2F.

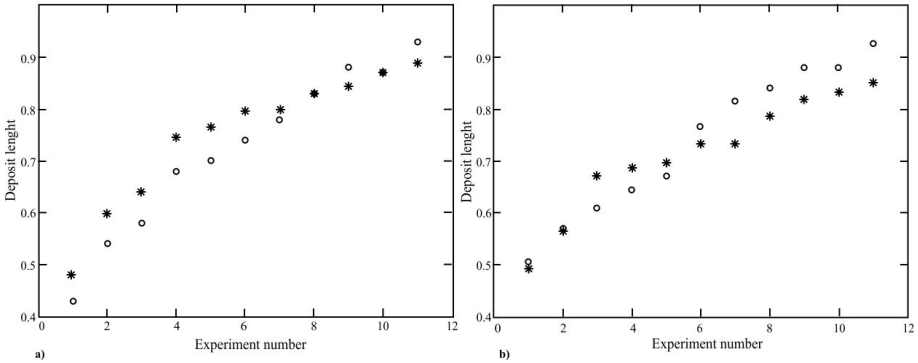

Abb. 3. Graphic comparison of the predictions of Titan2F for the experiments performed by Liu (1996). The results for several initial volumes compare **(a)** the width of the deposit and **(b)** the length of the deposit. The circles show data from the experiments, and the asterisks the predictions of Titan2F.

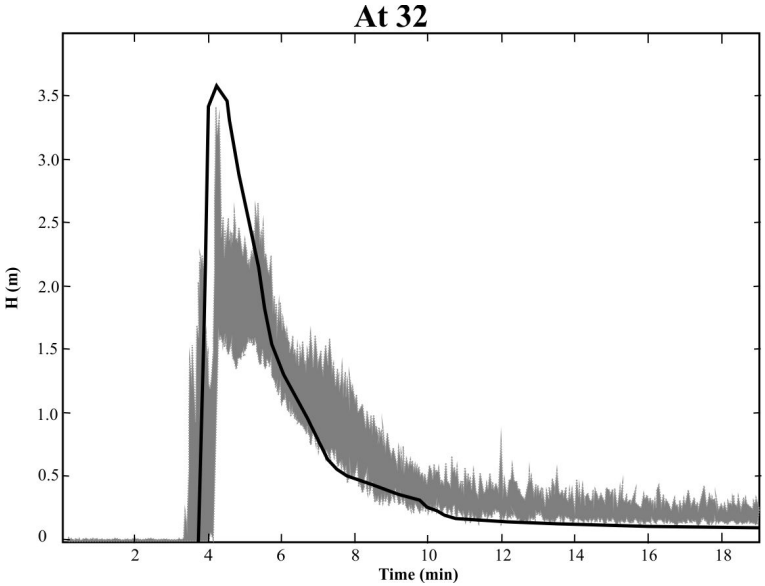

Abb. 4. Verification of the accuracy of the Titan2F predictions for the time evolution of the flow depth and arrival of the front at $32\,\mathrm{m}$ distance from the lock. The black line represents the Titan2F results. The gray shadowed interval represents the confidence interval of the experiments performed by Iverson and co-workers (Iverson et al., 2010).

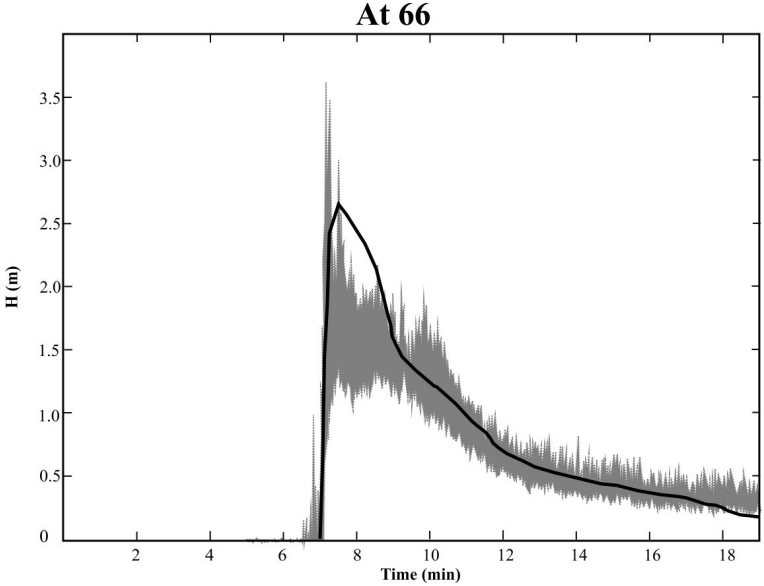

Abb. 5. Verification of the accuracy of the Two-Phase-Titan predictions for the time evolution of the flow depth and arrival of the front at $66\,\mathrm{m}$ distance from the lock. The black line represents the Titan2F results. The gray shadowed interval represents the confidence interval of the experiments performed by Iverson and co-workers (Iverson et al., 2010).

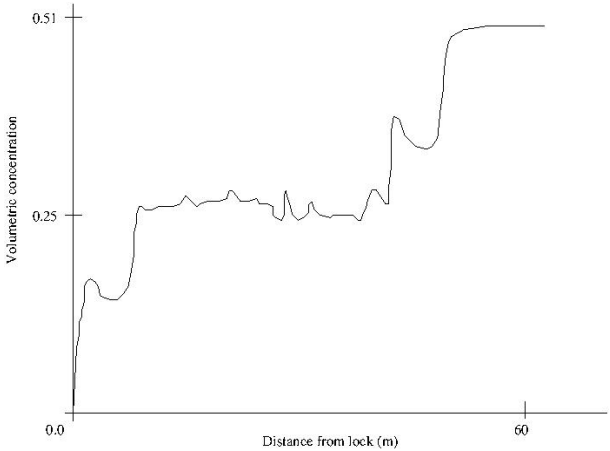

Abb. 6. Longitudinal distribution of the particle concentration after 14 s. The particle concentration at the upper part of the channel are very low, whereas at the end, the front of the flow becomes very concentrated, as observed by Iverson et al. (2010).

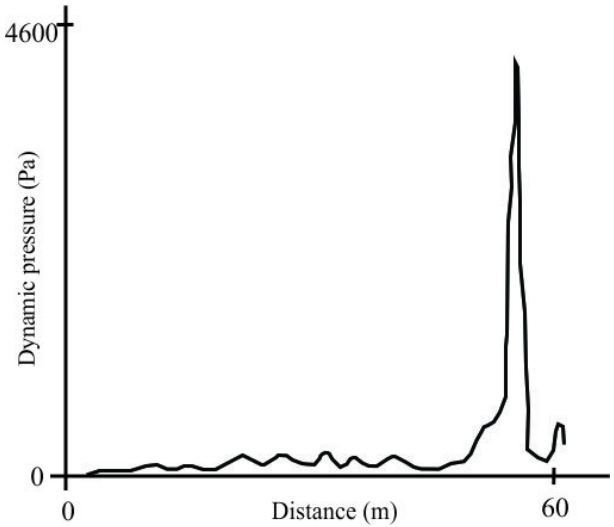

Abb. 7. Longitudinal distribution of the predicted dynamic pressure at 14s. The peak over-pressure occurs just at the end of the inclined part of the channel.